Identification of Agricultural Row Features Using Optical Data for Scattering and Reflectance Modeling Over Periodic Surfaces

Liujun Zhu, Jeffrey P. Walker, *Fellow, IEEE*, Christoph Rüdiger, *Senior Member, IEEE*, and Pengfeng Xiao, *Senior Member, IEEE*

***Abstract*—Various forward models have been developed for measuring agricultural biophysical parameters from the microwave or optical data, but their application to periodic surfaces (e.g., periodic crop rows and plowed soil rows) still suffers from the need of row-feature descriptions. Accordingly, an operational method was proposed herein to estimate the orientation and period of row features from very high spatial resolution optical data, as input to multi-scale scattering models. The periodic features were estimated from the frequency domain using the Fourier magnitude spectrum by scanning in azimuth to identify the presence/absence of periodic features and the main direction. The frequency representing the dominant periodic features was then determined from the main direction of the magnitude spectrum. Moreover, the tillage type of the bare soil surface was classified into one of three types (sinusoidal, sinusoidal bench, or bench) according to the magnitudes of dominant periodic features in the main direction. The method was evaluated using two data sets consisting of various agricultural features in regional Melbourne, Australia. The retrieval Root Mean Square Error (RMSE) in orientation and period was $< 3^\circ$ and 0.1 m. The overall accuracy of detecting the periodic features and tillage type classification was $>95\%$ and 70.59%, respectively. The proposed method and the retrieved periodic features are expected to partly solve the ill-posed nature of microwave data inversion over periodic surfaces.**

***Index Terms*—Agricultural row orientation, agricultural row period, high resolution optical data, multi-scale scattering model.**

I. Introduction

REMOTE sensing of agricultural biophysical parameters (e.g., biomass, soil roughness, soil moisture, and vegetation water content) is of tremendous scientific interest and practical value for solving the world's increasing demand of food. An isotropically rough surface and/or a uniform vegetation layer are commonly assumed, resulting in a few widely used classical scattering [1]–[3] and reflectance [4]–[6] models. However, this introduces large uncertainty in application to agricultural areas with periodic row features (e.g., periodic crop rows, plowed soil rows, and tracks from the agricultural machinery).

The effect of periodic row features on optical reflectance [7]–[9] and radar backscattering coefficient [10]–[14] and its subsequent applications have been demonstrated in many studies. For radar remote sensing, several papers have suggested the use of an effective roughness for periodic plowed surfaces [14]–[17], with the effective roughness parameterizations requiring further evaluation. A few multi-scale radar scattering models are available, including those developed for sinusoidal surfaces [1], [10], [18] and quasi-periodic rough surfaces [19]–[21]. Despite the root mean square height and correlation length describing the random roughness superimposed on the periodic surface, these models require the period, orientation, and the maximum height of the periodic surface, being more challenging to inverse using radar data only. Similarly, several optical radiative transfer models for row crops have been proposed [7], [22], [23], requiring the details of row features. In situ measurement of those parameters can be used for model development and validation. However, remote sensing of those periodic features for input to the scattering and reflectance models is more favorable from an operational perspective.

The agricultural row features present small-scale spatial heterogeneities in the landscape, as a result of cultivation activities (e.g., soil tillage, seeding, and harvesting), the variety of cultivated crops and varying growth patterns [24]. In radar images, the row structures observed perpendicular to the radar look direction have much larger co-polarized backscattering coefficient σ^0 (up to 10 dB) compared to those observed parallel to the radar look direction [12], [15], [25], [26], appearing as bright lines or curves within the fields. Similarly, oriented terrain features (mountain orientation) and urban structures have been found to have increased cross-polarization (HV) intensities and subsequently the coherency matrices become reflection asymmetric [27], with these changes detectable using polarimetric radars. Polarimetric decomposition methods were thus developed to roughly identify the orientation of large scale terrain features [27]–[29], with their application to determining the orientation of periodic features in agricultural fields being unresolved.

In optical data, furrows and crop rows are more straightforward and visible compared to that in radar data, being periodic lines or curves with a different reflectance. A great number of

Manuscript received December 10, 2019; revised March 22, 2020; accepted March 30, 2020. Date of publication April 17, 2020; date of current version May 4, 2020. The field data collection at Cora Lynn was supported by Australian Research Council Discovery Project DP170102373. *(Corresponding author: Liujun Zhu.)*

Liujun Zhu, Jeffrey P. Walker, and Christoph Rüdiger are with the Department of Civil Engineering, Monash University, Clayton, VIC 3800, Australia (e-mail: liujun.zhu@monash.edu; jeff.walker@monash.edu; chris.rudiger@monash.edu).

Pengfeng Xiao is with the Department of Geographic Information Science, Nanjing University, Nanjing, Jiangsu 210023, China (e-mail: xiaopf@nju.edu.cn).

Digital Object Identifier 10.1109/JSTARS.2020.2985506

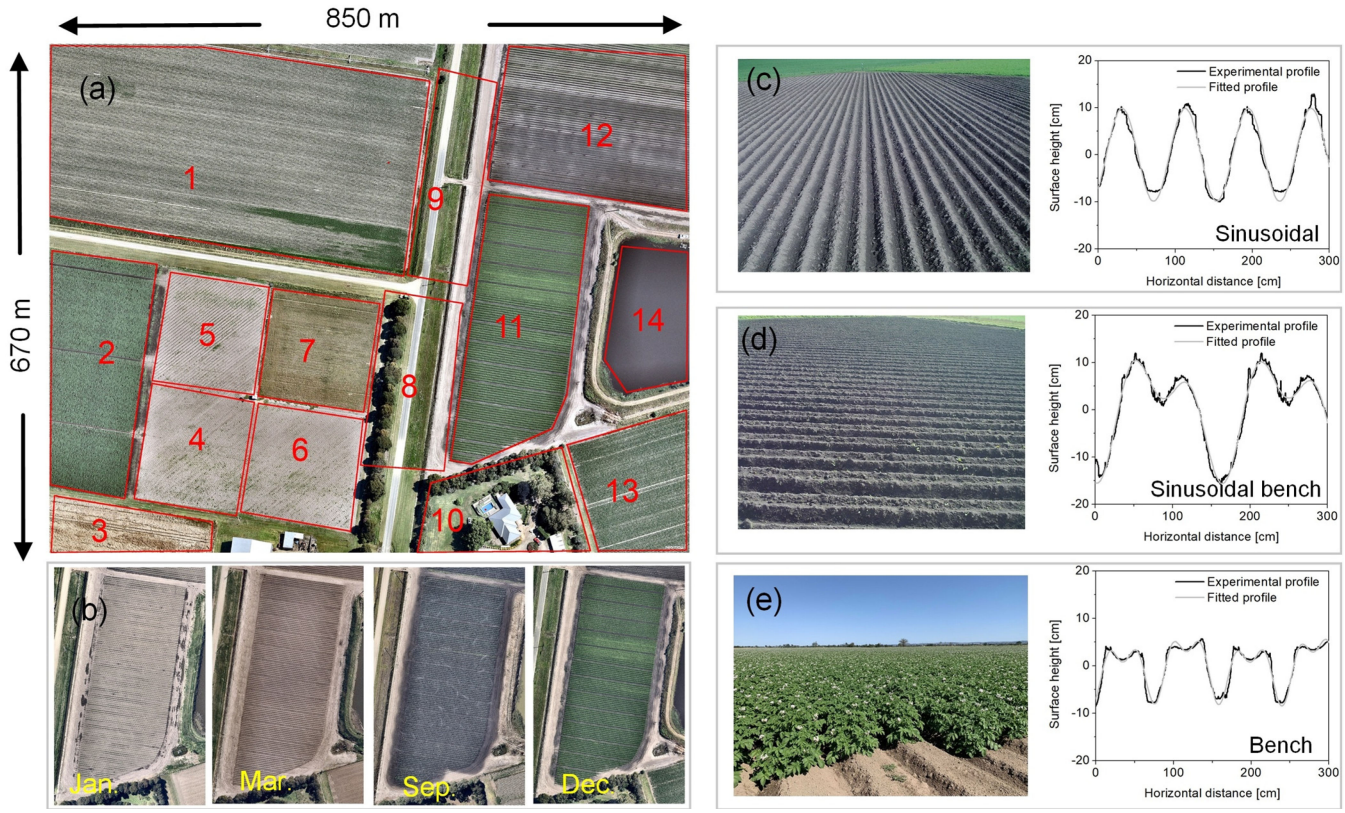

Fig. 1. Summary of the Cora Lynn site and collected data. (a) Image of the Cora Lynn site collected on December 24, 2018 as well as the paddock ID and boundaries for paddock scale analysis. (b) Multi-temporal images of paddock #11. (c)–(e) Images of three paddocks (#4, 5, and 2) with their experimental profiles measured in December 2018.

methods have been developed for detecting line features (e.g., road network, coastlines, and power line corridors) from optical data, with some those mostly encountered being the mathematical morphology methods [30]–[32] and classification-based methods [33]–[35]. These techniques have also been successfully applied to agricultural plots. For example, Sicre *et al.* [24] proposed a mathematical morphology algorithm for estimating crop azimuth using high resolution optical data (2 and 8 m), and various classifiers have been trained to determine the occurrence of tillage operations using SPOT-4 and ASAR data [36]. A more recent study applied the support vector machine together with various image features (spectrum, texture, and shape) to identify linear soil and water conservation structures [37]. While these methods can provide some valuable descriptions of agricultural line features, they are still insufficient for operational application to the aforementioned forward scattering models. At least two of the three periodic parameters (orientation, period, and maximum height) are required for inversion of these models using a single full-polarized radar acquisition.

To quantitatively measure these spatially small details, very high resolution (VHR) data is required. Fortunately, such data has become increasingly available over the past two decades, with recently launched commercial optical satellites (e.g., the Worldview series) achieving a spatial resolution of 0.3–0.5 m. While such high-resolution data may be acquired infrequently through time, they can still satisfy the requirement of forward models because the orientation and period of furrows and linear crop features remain constant throughout the same crop growth cycle.

In this study, an automatic method for estimating the orientation and period of soil tillage features and/or crop rows is presented. Accordingly, this method uses VHR optical imagery for the operational retrieval of biophysical parameters using available multi-scale scattering models. The method estimates these periodic features using Fournier magnitude spectrum, given the convenience of identifying periodic information in the frequency domain. Two data sets were used for the validation of the proposed method, being the remote sensing and ground data collected at a small focus area (Cora Lynn), and a regional data set collected in regional Melbourne, Australia.

II. Data Sets

A. Cora Lynn

The Cora Lynn study site is a flat agricultural area being 850 m by 670 m in size (Fig. 1(a)), located in regional Melbourne, Australia. A tower-based L/P-band radiometer system was setup in this area since November 2017 to demonstrate a new satellite concept of soil moisture mapping [38]. A total of 16 soil moisture monitoring stations were evenly distributed across this area, covering most of the typical land surface types, including wheat, corn, potato, grass, garlic, and lettuce. Intensive cultivation

TABLE I
GROUND MEASURED ROW FEATURES OF THE CORA LYNN SITE. THE TILLAGE TYPE 1, 2, AND 3 DENOTE THE SINUSOIDAL, SINUSOIDAL BENCH, AND BENCH, RESPECTIVELY

	Azimuth from north (°)				Period/Bench (m)				Tillage type			
#	Jan.	Mar.	Sep.	Dec.	Jan.	Mar.	Sep.	Dec.	Jan.	Mar.	Sep.	Dec.
1	-	-	-	101	-	-	-	0.75	-	-	-	-
2	-	80	-	99	-	3.63	-	0.92	-	3	-	-
3	110	111	-	-	0.7	0.74	-	-	-	-	-	-
4	-	-	55	55	-	-	0.90	0.90	-	-	1	1
5	-	-	54	54	-	-	1.80	1.80	-	-	2	2
6	-	-	55	55	-	-	0.90	0.90	-	-	1	1
7	-	-	-	-	-	-	-	-	-	-	-	-
8	-	-	-	-	-	-	-	-	-	-	-	-
9	-	-	-	-	-	-	-	-	-	-	-	-
10	-	-	-	-	-	-	-	-	-	-	-	-
11	96	96	96	96	1.50	1.50	1.50	1.50	3	3	3	3
12	100	100	100	100	1.50	1.50	1.50	1.50	3	3	3	3
13	-	75	-	75	-	0.75	-	0.75	-	2	-	2
14	-	-	-	-	-	-	-	-	-	-	-	-

activities (soil plowing, seeding, and harvest, etc.) were observed in 2018, resulting in regular changes of row orientation and periods. In particular, three paddocks (#4, #5, and #6) were plowed with periodic patterns and different orientations in July 2018 for analyzing the effect of row features on microwave observations.

Four of the available Nearmap images (https://www.nearmap.com.au) at the Cora Lynn site were used in this study; being the Red/Green/Blue images taken on January 19, March 28, September 5, and December 24, 2018, respectively, covering the main crop cycles in this area. The multi-temporal images of paddock #11 are included in Fig. 1(b) as an example. The first three images were dry to very wet bare soil surface, with the spray irrigation captured in the image of September. Dense lettuce was observed in December with clear periodic rows. The spatial resolution of these Nearmap images is 0.075 m, being much smaller than the period of the row features measured (Table I). Since the periodic row structure is uniform within a paddock, 13 paddocks were delineated using visual interpretation for analysis at the paddock scale.

Ground sampling of soil moisture, vegetation, and soil surface roughness were made in this area on a weekly-basis for the calibration/validation of soil moisture retrieval algorithms [38]. The orientation of crop and soil rows was measured using a compass, with the geomagnetic declination corrected. Soil surface profiles were also captured using a pin profiler over a length of 3 m, covering 2–4 periods for most paddocks. In general, the measured soil profiles could be classified into three types: sinusoidal, sinusoidal bench, and flat bench [39], with three corresponding examples (paddock #4, #5, and #2) shown in Fig. 1(c)–(e). These experimental profiles can be modeled as a sum of sinusoidal functions. One sinusoidal function (a component in frequency domain) was sufficient to represent one of the profile types shown in Fig. 1, while two and three sinusoidal functions were required for the bench-sinusoidal and bench types, respectively. Each sinusoidal function in the frequency domain is a bright point. Bare soil at the top part of the periodic surface commonly has lower soil moisture and subsequently higher reflectance in optical data (higher digital numbers in aerial images) than that at the bottom part as shown in Fig. 1(c). Moreover, the bottom parts may be covered by the shadow of the top parts, resulting in lower values in images. Accordingly, VHR images may provide valuable information of the soil vertical structures (e.g., the tillage type), required in microwave remote sensing applications [39], [40], although they do not directly measure the variation of surface height. The ground measured orientation and periods of crop and soil rows, and tillage type of bare soil paddocks are summarized in Table I. A total of 21 paddocks had periodic row features in the Cora Lynn data set, but covering only a narrow range of orientation (54°–110°) and periods (0.7–3.3 m). Accordingly, a larger data set with various row features was introduced for a more comprehensive validation.

B. Regional

The regional data set was selected from historic Nearmap images in regional Melbourne (Fig. 2), consisting of 200 separate images. Each image captured a homogeneous area with a size of 1000 × 1000 pixels. The main land cover of these images included bare soil, crop, grass, orchard, vineyard, water, residence, forest, and green house. Among these, the water body, residence, and forest were included as negative targets without periodic features, while the greenhouse provided testing on a more complex scenario. The linear features in grass images were mainly tracks of agricultural machinery and the residual grass after harvest as shown in Fig. 2, having irregular periodic features. The number of images with a periodic surface as a function of type are summarized in Fig. 2. Moreover, these images were roughly categorized into pure bare, sparsely vegetated area and fully covered vegetated area.

Ground measurements were not available for the historic images, but fortunately orientation and periods could be directly measured from the image itself and therefore used as the truth.

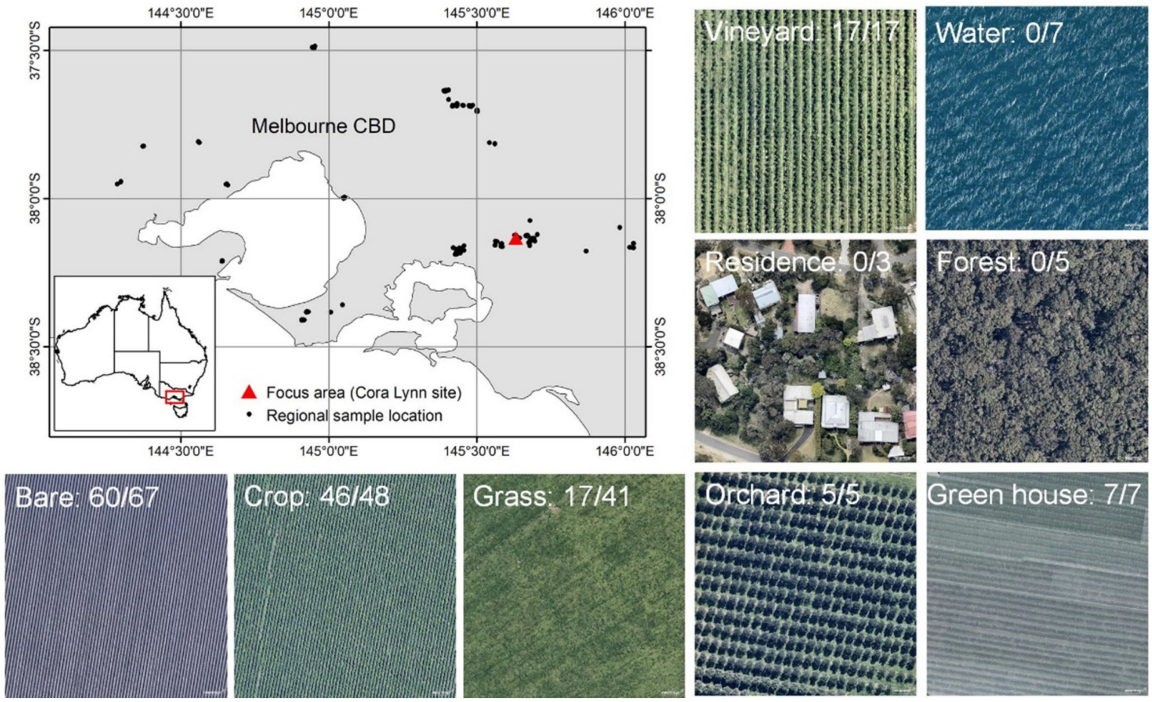

Fig. 2. Locations of the regional samples with examples of all land cover types included. The number A/B on the top of each example indicates the number of images with a periodic feature (A) and the total number of images for this category (B).

Specifically, the ruler tool in Photoshop was utilized to determine the period of rows in pixels and orientation in degrees. Ten evenly distributed measurements were made and averaged for each image, with each measurement including at least five periods. Measurements were also made for the Cora Lynn data set and compared with the ground measurements, showing a root mean square error (RMSE) of 5.6 cm in period and 0.82° in orientation, which was considered satisfactory for this study. The orientation of the regional data set covered the full range of angles between 0° and 180°, with most paddocks centered on 10°, 100°, 165°, and 180°. The measured periods also had a large range being ∼0.3–15 m, with the large values observed for periodic tracks. Notably, small periodic features may appear in crop paddocks (e.g., wheat rows can be 0.1–0.2 m), which can be hard to identify using the 0.075 m Nearmap images.

III. Methodology

A. Typical Agricultural Surfaces in the Frequency Domain

The characteristics of typical agricultural areas in the frequency domain were analyzed first. Only a brief introduction to the 2-D spectral analysis by Fourier transform is provided, as technique details [41] as well as applications to remote sensing images [42], [43] are already available in literature. Only square grey images were considered for simplicity, although the method also applies to rectangular images and a specific spectral band. Given an image $f(x, y)$ defined as an $N \times N$ array of grey-scale values in the range 0–255, the 2-D complex Fourier spectrum can be calculated by:

$$F(u,v) = \frac{1}{N^2} \sum_{x=0}^{N-1} \sum_{y=0}^{N-1} f(x,y) e^{-j2\pi(ux+vy)/N} \tag{1}$$

where u and v are wavenumbers representing the number of periods per image in the x and y directions respectively. The direct current component $F(0, 0)$ in the magnitude spectrum reflects the mean of the brightness of the original image. When expressed in polar form [41], the Fourier spectrum $F(r, \theta)$ can be explained by a weighted sum of cosine and sine waveforms, having varying spatial frequency $r = \sqrt{u^2 + v^2}$ and travelling direction $\theta = \tan^{-1}(u/v)$.

Several typical image examples and their magnitude spectrums ($|F(u, v)|$) in dB are presented in Fig. 3. Images with clear periodic soil row structures had a bright line in the magnitude spectrum, representing the significant periodic grey variation along the perpendicular direction of the row orientation. Moreover, there were several pairs of symmetric bright points on the bright line, denoting the dominant periodic structures in images. Accordingly, it is quite convenient to estimate the periods and orientation of agricultural rows using r and θ, after determination of the locations (u, v) of these bright points. The sinusoidal, sinusoidal bench, and bench type of bare soil had 1, 2, and 3 pairs of symmetric points respectively, in line with the experimental profiles in Fig. 1. The orchard example had periodic textures in multiple directions and thus contains multiple pairs of points in varying directions. In contrast, the two non-periodic examples (residential area and water) either had multiple bright lines

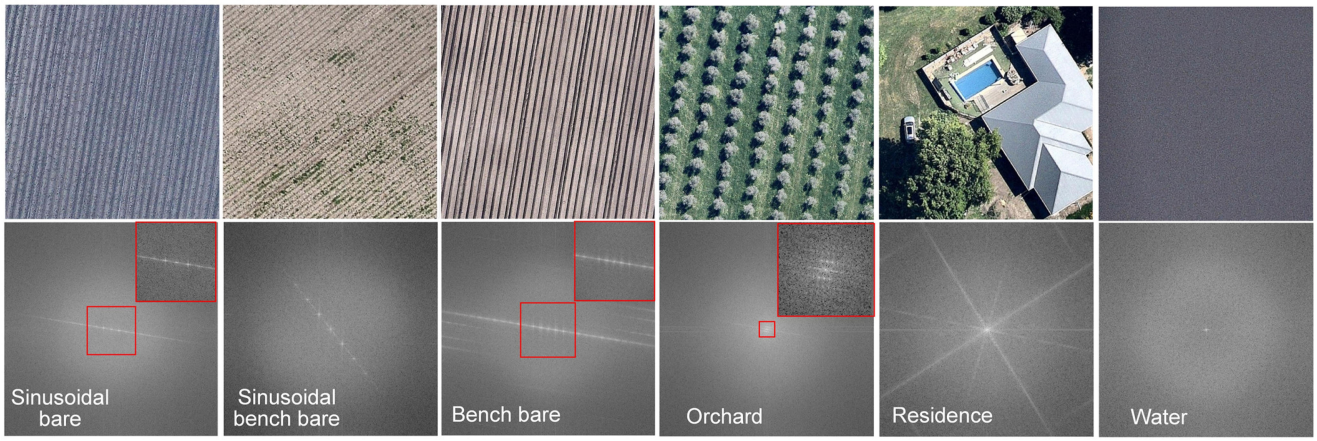

Fig. 3. Example images of agricultural areas and their magnitude spectrums in dB.

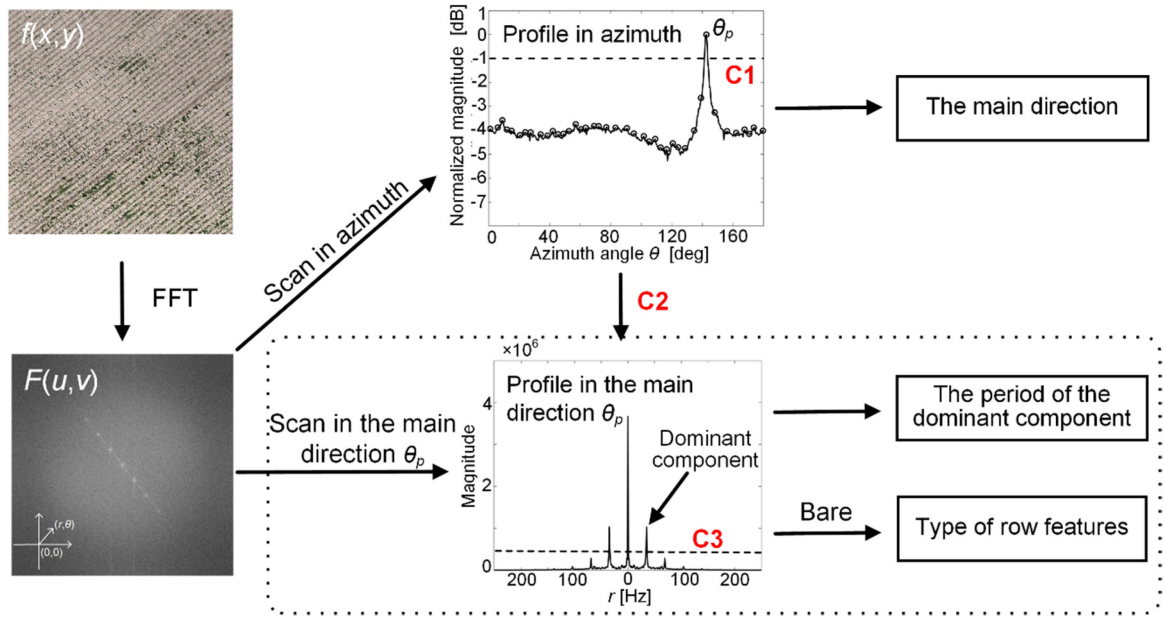

Fig. 4. Outline of the proposed method consisting of scanning in the azimuth and the main directions, with three criterions (C1, C2, and C3) proposed to determine row features.

without any clear points or no bright lines. The bright lines of the residential image resulted from the significant grey variations at the building's boundaries and have thus been used for image segmentation [44].

B. Proposed Method for Row Feature Estimation

Fig. 4 shows the outline of the proposed method, with the first step being the Fast Fournier Transform (FFT), followed by the two main steps to determine the locations representing the dominant periodic structures. Since the spectrum analysis based on the Fourier transform is a global technique, it can only provide the overall period and orientation of the whole image. Accordingly, a preprocessing step of image segmentation is required, with a number of sophisticated algorithms evaluated in Zhang *et al.* [45]. Alternatively, an image can be separated into several sub-images according to a uniform grid for a specific application, e.g., a soil moisture retrieval grid.

The angular distribution is first extracted by scanning in the azimuth from 0° to 180° with an interval of 0.5° [46]:

$$M(\theta) = \sum_{r=0}^{N/2} |F(r,\theta)| \tag{2}$$

where the scanning only applies to the circular area inscribed by the magnitude spectrum, and thus r has a maximum value of $N/2$. For areas with periodic features, the perpendicular direction (θ_p) of the dominant periodic features has the maximum magnitude value as described in Fig. 3. Accordingly, the orientation of the

rows (θ_{row}) can be calculated as:

$$\theta_{\text{row}} = \begin{cases} \theta_p - 90, \theta_p \geq 90 \\ \theta_p + 90, \theta_p < 90 \end{cases} \quad (3)$$

An example of the normalized angular distribution ($M(\theta)/M_{\max}$) in dB is shown in Fig. 4, with the maximum magnitude found at $\theta_p = 147°$ and thus the orientation of rows as 57°.

Areas with isotropic surfaces commonly have similar magnitudes in all directions (e.g., the spectrum of water in Fig. 3), meaning that multiple directions can have a similar value of $M(\theta_p)$. This was used to determine the presence/absence of periodic structures in this study. A threshold of −1 dB (∼0.79) was first applied to determine the number of orientations with a relatively large grey variation (dominant orientations), and images with more than three dominant orientations treated as isotropic (C2 in Fig. 4), because soil and crop rows within an agricultural paddock rarely have more than two orientations. Moreover, areas with periodic features in multiple directions will behave similarly to isotropic surfaces. The orchard in Fig. 3 is an example of a near isotropic surface. Notable is that anisotropic surfaces without periodic structures can also have multiple dominant orientations, as a result of the large grey variations at the boundaries of different land cover, e.g., the residence image in Fig. 3. Fortunately, most of those can be removed in the preprocessing stage of image segmentation, with patches having clear boundaries split into multiple sub-images.

For images with periodic structures, the magnitude profile $M(r, \theta_p)$ of the main direction θ_p was extracted. The $r_m(u_m, v_m)$ with the maximum magnitude excluding the direct current component $M(0, \theta_p)$ then was identified for estimating the period. As mentioned above, the frequency u_m and v_m denote the number of waveforms in the x and y directions, respectively. The period λ can thus be estimated as:

$$\lambda = |N \sin \theta_p / u_m|, \ 0 < \theta_p < 180° \quad (4)$$

or,

$$\lambda = |N \cos \theta_p / v_m|, \ \theta_p \neq 90° \quad (5)$$

where N is the size of the image. The identified u_m and v_m can also be used to update the $\theta_p = \tan^{-1}(u_m/v_m)$.

Despite the maximum magnitude at r_m, there are multiple peaks representing the minor periodic waveforms superimposed on the main waveform r_m. The number of those minor periodic waveforms can be related to the shape of the surface as depicted in Fig. 5. Despite the direct current component ($r = 0$), simulated sinusoidal, sinusoidal bench, and bench like surfaces (Fig. 5(a)) have 1, 2, and 3 peaks in the magnitude spectrum respectively (Fig. 5(b)), in line with the experimental magnitude spectrums of bare soil in Fig. 3. Fig. 5 also illustrates the limited contribution of the peaks outside the window of the bench type, because additional minor waveforms cannot have a substantial effect on the shape in the spatial domain. Accordingly, a threshold of the third peak' magnitude can be used to remove the waveforms with limited contributions. The theoretical normalized magnitude of the third peak of a rectangle signal is ∼0.0913 (C3 in Fig. 4). Accordingly, a peak with a normalized magnitude <0.0913 cannot have a significant effect on the shape of a surface. An image with 1, 2, and more than 2 dominant peaks in the magnitude spectrum was therefore determined as sinusoidal, sinusoidal bench, or bench type soil surface, respectively.

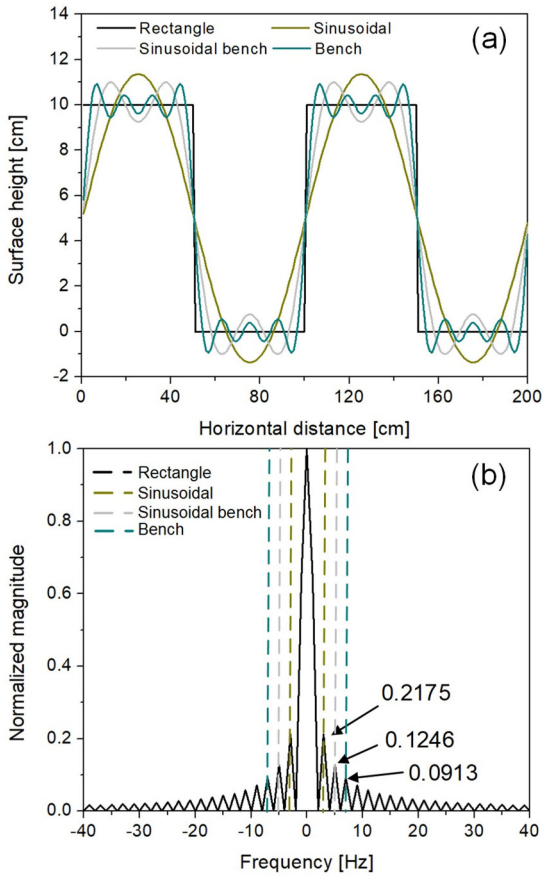

Fig. 5. Simulated rectangle signal and sinusoidal, sinusoidal bench, and bench surface in the (a) spatial and (b) frequency domain. The magnitude spectrums of sinusoidal, sinusoidal bench, and bench are those within the corresponding windows in (b), with the values outside the window (defined by peaks) being 0.

IV. Results and Discussions

A. Results of the Cora Lynn Site

The method was applied to the 4 images of the Cora Lynn site, taking the maximum rectangle area within each paddock as the input. The 21 paddocks with periodic features were successfully identified from a total of 56 paddocks, with 2 false alarms. These false alarms were paddock #7 (dense wheat) with a varying row spacing of ∼10–15 cm, which was not considered as a periodic feature during the ground sampling. This however confirms the capability of the proposed method and the VHR Nearmap data in capturing the tiny row features. Pearson's correlation (R), RMSE and bias were used to show the accuracy of orientation and period estimation below.

The estimated periods and orientation of the 21 identified paddocks (Table I) were compared with the ground measurements in Fig. 6. Satisfactory results ($R = 0.99$; RMSE = 2.17°) were achieved for orientation, being substantially better than that of a previous study (7.15° < RMSE < 43.02°) using 2-m

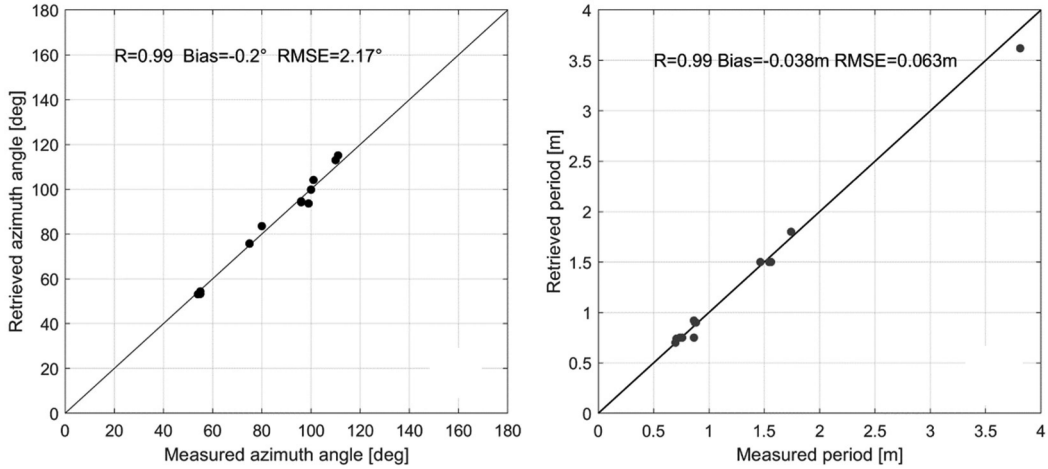

(a) (b)

Fig. 6. Ground measured against retrieved periodic features for the Cora Lynn site. (a) Azimuth angle. (b) Period.

TABLE II
PERFORMANCE USING DATA WITH DIFFERENT SPATIAL RESOLUTIONS

Spatial	Overall	Orientation [deg]			Period [m]		
Res. [cm]	Acc. [%]	R	Bias	RMSE	R	Bias	RMSE
7.5	96.4	0.99	-0.2	2.17	0.99	-0.04	0.06
15	96.4	0.98	-1.87	3.1	0.95	-0.05	0.08
30	94.6	0.98	-1.91	3.09	0.89	0.04	0.12
60	**64.3**	0.97	3.04	4.1	**0.05**	**1.01**	**1.88**

TABLE III
ERROR MATRIX OF IDENTIFYING TILLAGE TYPE OF BARE SOIL SURFACES

Classified	Ground measured		
	Sinusoidal	Sinusoidal bench	Bench
Sinusoidal	3	0	0
Sinusoidal bench	2	2	2
Bench	0	1	7

Formosat-2 data [24]. However, the major improvement may come from the use of much higher resolution data in this study, because it is more challenging to identify the line features in a coarser image as shown in the further analysis presented below. The retrieved period had an R and RMSE of 0.99 and 0.063 m respectively, suggesting the best accuracy that can be achieved from the Nearmap data because the RMSE is already smaller than the 0.075 m spatial resolution of the data used. The crop coverage (0% to $\sim$100%) and the irrigation observed at paddock #11 (Fig. 1) had no effect on the retrieval results as clear linear features could still be observed and identified using the proposed method.

The relationship between spatial resolution and the performance is summarized in Table II. The data with resolutions of 0.15, 0.3, and 0.6 m were resampled from the 0.075-m data using cubic convolution interpolation. The proposed method had similar performance for resolutions less than 0.6 m, but had a significant deterioration using the 0.6-m data. The overall accuracy of periodic surface identification using the 0.6-m data was only 64.3% and the RMSE of period retrieval was 1.88 m, being larger than the periods of most paddocks in the Cora Lynn site. This can be explained by the Nyquist Sampling Theorem which suggests a minimum sample rate requirement of twice that of the signal frequency. The periods of 9 paddocks ($<$1 m) in the Cora Lynn data set were smaller than two pixels (1.2 m) using the 0.6-m data, resulting in poor retrieval. More importantly, the Nyquist Sampling Theorem also suggests that VHR images with a resolution of $\sim$0.3 m from satellites (e.g., the Wordview series) are sufficient for the extraction of line features with a period of $>$ 0.6 m.

Table III shows the error matrix of tillage type classification, with an overall accuracy of 70.59%. This is better than the results (23%–60%) reported in Colpitts [40] using C-band RADARSAT-1 data where four tillage types were included. Not surprisingly, all misclassifications were observed between the sinusoidal bench and the other two types, because the sinusoidal bench is the intermediate type between sinusoidal and bench types. Those misclassifications may not be removed using optical data considering the non-straightforward relationship between soil surface shape and the grey variation across rows. The soil moisture variation in the soil surface profile and shadows can introduce large uncertainty on the grey profile in optical data, being difficult to be measured quantitatively. Moreover, the physical soil profiles also undergo a smoothing process after the tillage, resulting in an intermediate status of sinusoidal bench and bench.

Despite the applications at the paddock scale, the proposed method also applies to sub-images split by a uniform grid, which can be the subsequent application grid, e.g., the radar data grid for soil moisture retrieval. The image depicted in Fig. 1 was used to investigate the performance at uniform grids of 10, 30, and 50 m, with a focus on the effect of mixed pixel or grid. In general, the retrieved periods and orientation of the three grid resolutions agreed well with the ground measurements (Fig. 7). False alarms were observed in paddock #7 at 10 and 30 m, coincident with the results retrieved at the paddock scale. Additional false alarms

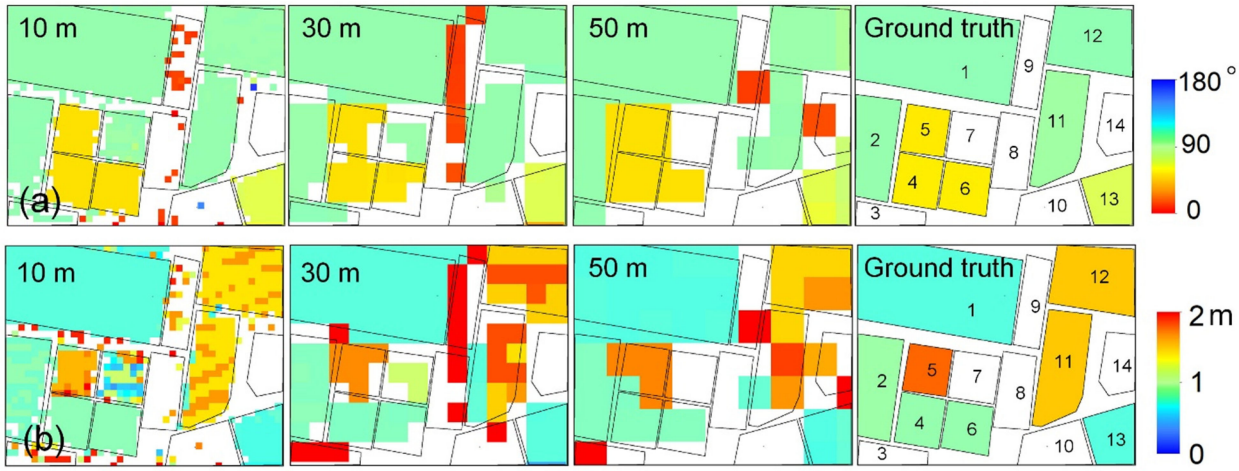

Fig. 7. Retrieved (a) azimuth angle and (b) period when analyzing on regular grids of 10, 30, and 50 m rather than paddocks.

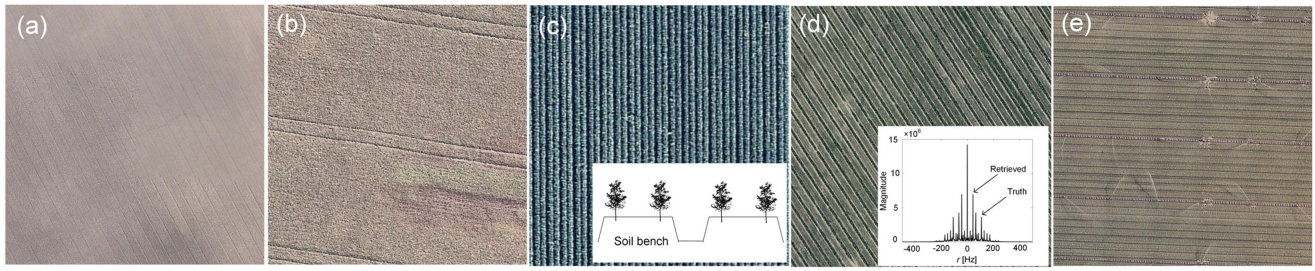

Fig. 8. Examples of images erroneously identified or measured by the proposed method. (a) and (b) Two examples of omission error. (c)–(e) Cases with erroneous periods.

were found in paddocks #3, #8, and #9, as a result of the line texture contained in these paddocks (Fig. 1). At the 10-m grid retrieval, substantial omissions occurred at the boundaries (mixed pixels) of most paddocks although the major parts of some mixed pixels had periodic rows. This was slightly worse for the 30- and 50-m grid retrievals, especially for paddock #6 and #11. Moreover, the mixed pixel also resulted in uncertainties for the period estimation. For example, the boundary pixels of paddock #11 had a retrieved period of 0.7–1.96 m when the grid size was 30 or 50 m. This may suggest the use of a grid with high resolution first and then upscaled to the target grid of the subsequent applications, although a small grid size may not capture the row feature with a large period.

B. *Results of the Regional Set*

When applied to the regional data set the proposed method missed 8 paddocks with periodic features from the 200 paddocks tested, without any false alarms. Thus, the overall accuracy was 96%. The missed paddocks can be roughly classified into two categories. The first class (3 paddocks) had a shallow plowing depth, being similar to the isotropic surface (see Fig. 8(a) for an example). The periodic linear features in the second class (4 paddocks) were tracks of irrigation booms (Fig. 8(b)). These paddocks had a relatively large period ($\sim$30 m) separated by 2 narrow tracks ($<$1 m) caused by the two wheels of the irrigation booms. The magnitude of the highest component of these paddocks was $<$ 2% of the direct current component because of the small grey variation across the rows. As a result, these paddocks were erroneously identified as an isotropic surface.

The estimated orientation and periods of the identified 136 paddocks were compared with the measured truth in Fig. 9. Similar to the results of Cora Lynn, the R and RMSE of the retrieved row orientation was 0.99° and 0.86°, respectively, confirming the effectiveness of the proposed method in a wide range of agricultural areas. Similar results were achieved for images with pure bare soil, sparse vegetation and fully covered vegetation. Non-periodic sparse vegetation has a limited effect on the point representing the main periodic features in the frequency domain, e.g., the example in Fig. 4.

The retrieved periods of 11 paddocks were nearly twice or three times of the measured truth, while the periods of 3 paddocks were half of the truth. Among these, the error of 9 paddocks related to the definition of period. There are two kinds of periodic features in arable regions (crop rows and soil rows) (Fig. 8(c)). The soil rows are the main periodic features in the early stage of crops, while crops become dominant after the presence of vegetation. For major crop paddocks, the period of soil rows can be twice that of the period of crop rows as per the example in Fig. 8(c), resulting in the error presented in Fig. 9.

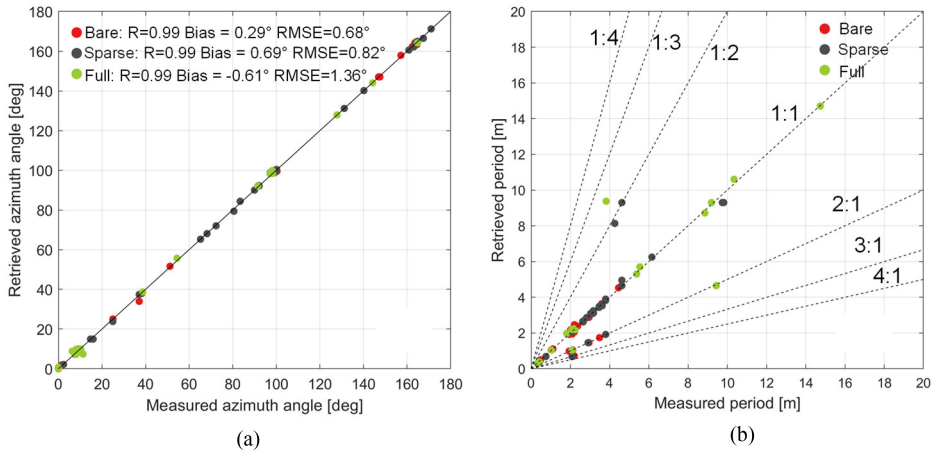

Fig. 9. Ground measured (a) azimuth angle and (b) period against retrieved periodic features for the regional data site. The Bare, Sparse and Full refers to images with pure bare soil, sparse vegetation and fully covered vegetation, respectively.

The other reason is that the peak representing the measured period is not the maximum in the magnitude spectrum. This was observed in paddocks with bench-like surfaces (Fig. 8(d)) or multiple periodic structures caused by the irrigation system (Fig. 8(e)), where multiple peaks with similar magnitudes can be found in the magnitude spectrum. Since the periods of all the peaks can be estimated (4) and (5), *a prior* knowledge of the period range can help to select the one close to the truth. For example, the periods of arable land are commonly <2 m in both data sets and thus peaks representing a period >2 m can be removed.

V. Conclusion

An operational method to determine the row orientation, period, and the tillage types of bare soil within paddocks was presented, being the inputs required for scattering models. The spectrum in the frequency domain was used to quantitatively extract the periodic features with two conventional steps and three thresholds, rather than complex geometry measures in the spatial domain. Despite the proposed thresholds, the method can be implemented in an entirely unsupervised way for orientation and period extraction.

Two data sets were used to evaluate the performance of the proposed methods, showing an overall accuracy of $>95\%$ in detecting the periodic features. The retrieval error (RMSE) in orientation and period is $<3^\circ$ and 0.1 m in both data sets excluding the uncertainty caused by the definition of period over arable lands. Satisfactory overall accuracy (70.59%) of tillage type classification was achieved, considering the poor relationship between grey variation in images and soil surface profile. However, more ground measurements of tillage types were required for a further evaluation.

The effect of spatial resolution was investigated using the Cora Lynn data set, demonstrating the effectiveness of using VHR data from available satellites over a larger area. For small area applications requiring prompt updates, the Unmanned Aerial Vehicles (UAVs) based optical sensors provide a promising alternative. The proposed method was also applied to images split into uniform grids with satisfactory results, providing a convenient preprocessing step for backscatter prediction and geophysical parameter retrieval. The method can provide two of the five unknowns (row orientation, row period, maximum height, RMS height and correlation length) required in multi-scale surface scattering models (e.g., [1], [18], and thus soil moisture retrieval can be conducted using full polarized radar data (three independent radar measurements).

References

[1] A. K. Fung, *Microwave Scattering and Emission Models and Their Applications*. Norwood, MA, USA: Artech House, 1994.
[2] E. Attema and F. T. Ulaby, "Vegetation modeled as a water cloud," *Radio Sci.*, vol. 13, no. 2, pp. 357–364, 1978.
[3] R. H. Lang and J. S. Sighu, "Electromagnetic backscattering from a layer of vegetation: A discrete approach," *IEEE Trans. Geosc. Remote Sens.*, vol. 21, no. 1, pp. 62–71, 1983.
[4] G. H. Suits, "The calculation of the directional reflectance of a vegetative canopy," *Remote Sens. Environ.*, vol. 2, pp. 117–125, 1971.
[5] Q. Wenhan and D. L. Jupp, "An analytical and computationally efficient reflectance model for leaf canopies," *Agricultural Forest Meteorol.*, vol. 66, no. 1–2, pp. 31–64, 1993.
[6] A. Kuusk, "A fast, invertible canopy reflectance model," *Remote Sens. Environ.*, vol. 51, no. 3, pp. 342–350, 1995.
[7] F. Zhao *et al.*, "A spectral directional reflectance model of row crops," *Remote Sens. Environ.*, vol. 114, no. 2, pp. 265–285, 2010.
[8] M. O. Román, C. K. Gatebe, C. B. Schaaf, R. Poudyal, Z. Wang, and M. D. King, "Variability in surface BRDF at different spatial scales (30 m–500 m over a mixed agricultural landscape as retrieved from airborne and satellite spectral measurements," *Remote Sensing Environ.*, vol. 115, no. 9, pp. 2184–2203, 2011.
[9] G. Yan *et al.*, "Review of indirect optical measurements of leaf area index: Recent advances, challenges, and perspectives," *Agricultural Forest Meteorol.*, vol. 265, pp. 390–411, 2019.
[10] A. Monsivais-Huertero, P.-W. Liu, and J. Judge, "Phenology-based backscattering model for corn at L-band," *IEEE Trans. Geosci. Remote Sens.*, vol. 56, no. 9, pp. 4989–5005, Feb. 2018.
[11] M. Whitt and F. Ulaby, "Radar response of periodic vegetation canopies," *Int. J. Remote Sens.*, vol. 15, no. 9, pp. 1813–1848, 1994.
[12] M. Zribi, O. Taconet, V. Ciarletti, and D. Vidal-Madjar, "Effect of row structures on radar microwave measurements over soil surface," *Int. J. Remote Sens.*, vol. 23, no. 24, pp. 5211–5224, 2002.
[13] U. Wegmüller *et al.*, "Progress in the understanding of narrow directional microwave scattering of agricultural fields," *Remote Sens. Environ.*, vol. 115, no. 10, pp. 2423–2433, 2011.

[14] L. Zhu, J. P. Walker, L. Tsang, H. Huang, N. Ye, and C. Rüdiger, "Soil moisture retrieval from time series multi-angular radar data using a dry down constraint," *Remote Sens. Environ.*, vol. 231, 2019, Art. no. 111237.
[15] I. Champion and R. Faivre, "The field row direction relative to the radar azimuth considered as an apparent surface roughness for smooth bare soils," *Int. J. Remote Sens.*, vol. 17, no. 16, pp. 3305–3311, 1996.
[16] A. Joseph, R. van der Velde, P. O'Neill, R. Lang, and T. Gish, "Effects of corn on C-and L-band radar backscatter: A correction method for soil moisture retrieval," *Remote Sens. Environ.*, vol. 114, no. 11, pp. 2417–2430, 2010.
[17] L. Zhu, J. P. Walker, L. Tsang, H. Huang, N. Ye, and C. Rüdiger, "A multi-frequency framework for soil moisture retrieval from time series radar data," *Remote Sens. Environ.*, vol. 235, 2019, Art. no. 111433.
[18] F. T. Ulaby, F. Kouyate, A. K. Fung, and A. J. Sieber, "A backscatter model for a randomly perturbed periodic surface," *IEEE Trans. Geosci. Remote Sens.*, vol. GE-20, no. 4, pp. 518–528, 1982.
[19] R. Shin and J. Kong, "Scattering of electromagnetic waves from a randomly perturbed quasiperiodic surface," *J. Appl. Phys.*, vol. 56, no. 1, pp. 10–21, 1984.
[20] F. Mattia, "Coherent and incoherent scattering from tilled soil surfaces," *Waves Random Complex Media*, vol. 21, no. 2, pp. 278–300, 2011.
[21] F. Mattia and T. Le Toan, "Backscattering properties of multi-scale rough surfaces," *J. Electromagn. Waves Appl.*, vol. 13, no. 4, pp. 493–527, 1999.
[22] G. H. Suits, "Extension of a uniform canopy reflectance model to include row effects," *Remote Sens. Environ.*, vol. 13, no. 2, pp. 113–129, 1983.
[23] A. Ganis, "Radiation transfer estimate in a row canopy: A simple procedure," *Agricultural Forest Meteorol.*, vol. 88, no. 1-4, pp. 67–76, 1997.
[24] C. M. Sicre, F. Baup, and R. Fieuzal, "Determination of the crop row orientations from Formosat-2 multi-temporal and panchromatic images," *ISPRS J. Photogrammetry Remote Sens.*, vol. 94, pp. 127–142, 2014.
[25] B. Blanchard and A. Chang, "Estimation of soil moisture from Seasat SAR data," *J. Amer. Water Resources Assoc.*, vol. 19, no. 5, pp. 803–810, 1983.
[26] F. T. Ulaby and J. Bare, "Look direction modulation function of the radar backscattering coeffieient of agricultural fields," *Photogrammetric Eng. Remote Sens.*, vol. 45, no. AP11, pp. 1495–1506, Nov. 1979.
[27] J.-S. Lee, D. L. Schuler, and T. L. Ainsworth, "Polarimetric SAR data compensation for terrain azimuth slope variation," *IEEE Trans. Geosc. Remote Sens.*, vol. 38, no. 5, pp. 2153–2163, Sep. 2000.
[28] J.-S. Lee, D. L. Schuler, T. L. Ainsworth, E. Krogager, D. Kasilingam, and W.-M. Boerner, "On the estimation of radar polarization orientation shifts induced by terrain slopes," *IEEE Trans. Geosci. Remote Sens.*, vol. 40, no. 1, pp. 30–41, Jan. 2002.
[29] A. Bhattacharya, A. Muhuri, S. De, and A. C. Frery, "Orientation angle estimation from PolSAR data using a stochastic distance," in *Proc. IEEE Geosci. Remote Sens. Symp.*, 2014, pp. 3474–3477.
[30] C. Zhu, W. Shi, M. Pesaresi, L. Liu, X. Chen, and B. King, "The recognition of road network from high-resolution satellite remotely sensed data using image morphological characteristics," *Int. J. Remote Sens.*, vol. 26, no. 24, pp. 5493–5508, 2005.
[31] S. Valero, J. Chanussot, J. A. Benediktsson, H. Talbot, and B. Waske, "Advanced directional mathematical morphology for the detection of the road network in very high resolution remote sensing images," *Pattern Recognit. Lett.*, vol. 31, no. 10, pp. 1120–1127, 2010.
[32] L. Courtrai and S. Lefèvre, "Morphological path filtering at the region scale for efficient and robust road network extraction from satellite imagery," *Pattern Recognit. Lett.*, vol. 83, pp. 195–204, 2016.
[33] M. Mokhtarzade and M. V. Zoej, "Road detection from high-resolution satellite images using artificial neural networks," *Int. J. Appl. Earth Observ. Geoinformation*, vol. 9, no. 1, pp. 32–40, 2007.
[34] I. Grinias, C. Panagiotakis, and G. Tziritas, "MRF-based segmentation and unsupervised classification for building and road detection in peri-urban areas of high-resolution satellite images," *ISPRS J. Photogrammetry Remote Sens.*, vol. 122, pp. 145–166, 2016.
[35] Z. Zhang, Q. Liu, and Y. Wang, "Road extraction by deep residual U-Net," *IEEE Geosci. Remote Sens. Lett.*, vol. 15, no. 5, pp. 749–753, 2018.
[36] E. Vaudour, N. Baghdadi, and J.-M. Gilliot, "Mapping tillage operations over a peri-urban region using combined SPOT4 and ASAR/ENVISAT images," *Int. J. Appl. Earth Observ. Geoinformation*, vol. 28, pp. 43–59, 2014.
[37] S. Eckert, S. T. Ghebremicael, H. Hurni, and T. Kohler, "Identification and classification of structural soil conservation measures based on very high resolution stereo satellite data," *J. Environ. Manage.*, vol. 193, pp. 592–606, 2017.
[38] N. Ye *et al.*, "Towards multi-frequency soil moisture retrieval using P-and L-band passive microwave sensing technology," in *Proc. IGARSS 2018-2018 IEEE Int. Geosci. Remote Sens. Symp.*, 2018, pp. 3707–3710.
[39] Y. Gao, "Joint active passive microwave soil moisture retrieval," Ph.D. dissertation, Dept. Civil Eng., Monash Univ., Clayton, VIC, Australia, 2016. [Online]. Available: http://users.monash.edu. au/∼ jpwalker/theses/YingGao. pdf
[40] B. G. Colpitts, "The integral equation model and surface roughness signatures in soil moisture and tillage type determination," *IEEE Trans. Geosci. Remote Sens.*, vol. 36, no. 3, pp. 833–837, May 1998.
[41] R. N. Bracewell and R. N. Bracewell, *The Fourier Transform and Its Applications*. New York: McGraw-Hill, 1986.
[42] P. Couteron, R. Pelissier, E. A. Nicolini, and D. Paget, "Predicting tropical forest stand structure parameters from Fourier transform of very high-resolution remotely sensed canopy images," *J. Appl. Ecology*, vol. 42, no. 6, pp. 1121–1128, 2005.
[43] D. Rocchini, M. Metz, C. Ricotta, M. Landa, A. Frigeri, and M. Neteler, "Fourier transforms for detecting multitemporal landscape fragmentation by remote sensing," *Int. J. Remote Sens.*, vol. 34, no. 24, pp. 8907–8916, 2013.
[44] P. Xiao, X. Feng, R. An, and S. Zhao, "Segmentation of multispectral high-resolution satellite imagery using log gabor filters," *Int. J. Remote Sens.*, vol. 31, no. 6, pp. 1427–1439, 2010.
[45] X. Zhang, X. Feng, P. Xiao, G. He, and L. Zhu, "Segmentation quality evaluation using region-based precision and recall measures for remote sensing images," *ISPRS J. Photogrammetry Remote Sens.*, vol. 102, pp. 73–84, 2015.
[46] R. W. Conners and C. A. Harlow, "A theoretical comparison of texture algorithms," *IEEE Trans. Pattern Anal. Mach. Intell.*, vol. 2, no. 3, pp. 204–222, Mar. 1980.

Liujun Zhu received the B.S. degree in geography from Zhejiang Normal University, Jinhua, China, in 2012, and the M.Sc. degree in geography information science from Nanjing University, Nanjing, China, in 2015. He obtained the Ph.D. degree in civil engineering, in 2019 from Monash University, Melbourne, VIC, Australia, with a thesis on multi-SAR soil moisture retrieval. During 2017–2018, he was a visiting Ph.D. student with the University of Michigan-Ann Arbor, Ann Arbor, MI, USA. Since 2019, he has been a Research Fellow with Monash University, continuing research on radar soil moisture. His current research interests include microwave remote sensing of soil moisture, machine learning and its applications in soil moisture, and live fuel water content retrieval.

Jeffrey P. Walker (Fellow, IEEE) received the B.E. (Civil) and B.Surveying degrees in 1995 with hons 1 and university medal from the University of Newcastle, Australia, and his Ph.D. in water resources engineering from the same University, in 1999. His Ph.D. dissertation was among the early pioneering research on estimation of root-zone soil moisture from assimilation of remotely sensed surface soil moisture observations. Then, he joined NASA Goddard Space Flight Centre to implement his soil moisture work globally. He was a Lecturer with the Department of Civil and Environmental Engineering, University of Melbourne, in 2019, where he continued his soil moisture work, including development of the only Australian airborne capability for simulating new satellite missions for soil moisture. Since 2010, he is a Professor with the Department of Civil Engineering, Monash University, Melbourne, VIC, Australia, where he is continuing this research. He is contributing to soil moisture satellite missions at NASA, Washington, DC, USA, ESA, Paris, France, and JAXA, Tokyo, Japan, as a science team member for the Soil Moisture Active Passive Mission and Cal/Val Team member for the Soil Moisture and Ocean Salinity and the Global Change Observation Mission—Water, respectively.

Christoph Rüdiger (Senior Member, IEEE) received the B.E. (Civil) from Germany and the Ph.D. degree in environmental engineering from the University of Melbourne. He began his research career working for the French Bureau of Meteorology and Space Agency to evaluate the quality of soil moisture products observed from space and to prepare their inclusion into the French land service prediction system. He returned to Australia in 2008 to coordinate a number of field campaigns for the Australian land validation segment of the first global soil moisture satellite mission across the Australian arid zone and the Murrumbidgee River catchment. He has been a faculty member with the Department of Civil Engineering at Monash University (Melbourne, Australia) since 2011 and the Director of the Monash AgTech Launchpad since early 2019. His current research interests include satellite-based monitoring of land surface dynamics to assess droughts and agricultural activities, as well as wildfire predictions

Pengfeng Xiao (Senior Member, IEEE) was born in Hunan, China, in 1979. He received the B.M. degree in land resource management from Hunan Normal University, Changsha, China, in 2002, and the Ph.D. degree in cartography and geographical information system from Nanjing University, Nanjing, China, in 2007. From 2007 to 2009, he was a Lecturer in the School of Geography and Ocean Science at Nanjing University, where he was an Associate Professor from 2010 to 2018. Since 2019, he has been a Professor with Nanjing University. He was a Visiting Scholar with the Department of Geography, University of Giessen, Giessen, Hesse, Germany, from 2011 to 2012, and with the Department of Environmental Science, Policy, and Management, University of California at Berkeley, Berkeley, California, USA, from 2014 to 2015. He has authored over 60 articles. His current research interests include remote sensing image processing, land use and land cover change, and remote sensing of snow cover.